HHS Public Access

Author manuscript

ASAIO J. Author manuscript; available in PMC 2020 June 14.

Published in final edited form as:

ASAIO J. 2020 April ; 66(4): 423–432. doi:10.1097/MAT.0000000000001018.

Low-Resistance, Concentric-Gated Pediatric Artificial Lung for End-Stage Lung Failure

Alex J. Thompson[*], **Skylar Buchan**[*], **Benjamin Carr**[*], **Clinton Poling**[*], **McKenzie Hayes**[*], **Uditha Piyumindri Fernando**[*], **Andreas Kaesler**[†], **Peter Schlanstein**[†], **Felix Hesselmann**[†], **Jutta Arens**[†], **Joseph A. Potkay**[*], **Alvaro Rojas-Peña**[*], **Robert H. Bartlett**[*], **Ronald B. Hirschl**[*]

[*]Extracorporeal Life Support Laboratory, Department of Surgery, University of Michigan, Ann Arbor, Michigan;

[†]Department of Cardiovascular Engineering, Institute of Applied Medical Engineering, Helmholtz Institute, RWTH Aachen University, Aachen, Germany.

Abstract

Children with end-stage lung failure awaiting lung transplant would benefit from improvements in artificial lung technology allowing for wearable pulmonary support as a bridge-to-transplant therapy. In this work, we designed, fabricated, and tested the Pediatric MLung—a dual-inlet hollow fiber artificial lung based on concentric gating, which has a rated flow of 1 L/min, and a pressure drop of 25 mm Hg at rated flow. This device and future iterations of the current design are designed to relieve pulmonary arterial hypertension, provide pulmonary support, reduce ventilator-associated injury, and allow for more effective therapy of patients with end-stage lung disease, including bridge-to-transplant treatment.

Keywords

extracorporeal life support; hollow fiber oxygenator; wearable artificial lung

One in five children with end-stage lung failure (ESLF) die while awaiting transplant.[1] Hollow fiber oxygenators or artificial lungs (ALs) are commonly used to provide pulmonary support in acute and bridge-to-transplant applications. In these devices, blood flows around a bundle of hollow fibers, while a sweep gas supplied to the fibers' lumens facilitates gas transfer *via* diffusion through the fiber wall. The benefits of a particular AL depend on the design properties and engineering of the AL, and device development must be thoughtfully targeted to the intended patient population to achieve optimal results. In this work, we design, fabricate, and test the performance of a paracorporeal, pumpless device intended for pediatric patients. This device, called the "Pediatric MLung," can be used as a bridge to transplant for children with ESLF.

Correspondence: Alex J. Thompson, VA Ann Arbor Healthcare System, Bldg 22 Room G08, 2215 Fuller Rd, Ann Arbor, MI 48105. ajthomp@umich.edu.

Disclosure: The authors have no conflicts of interest to report.

Supplemental digital content is available for this article. Direct URL citations appear in the printed text, and links to the digital files are provided in the HTML and PDF versions of this article on the journal's Web site (www.asaiojournal.com).

The Pediatric MLung (Extracorporeal Life Support Lab, University of Michigan, Ann Arbor, Michigan) is designed to be attached *via* a pulmonary artery (PA) to left atrium (LA) configuration. The PA–LA configuration is advantageous because it is attached in parallel to the native lung, such that high pressure in the right ventricle (RV) is relieved due to the availability of a flow path of lower resistance.[2] Additionally, the PA–LA configuration provides a pressure gradient for device blood flow, so that it can be operated without a blood pump. This configuration has been demonstrated previously[3–7]; however, improvements in the technology are needed because mortality rates remain high due to clot formation and stroke caused by inefficiencies in AL configuration and flow. Development of smaller, more efficient devices is advantageous because reduction of priming volume and blood-contacting surface area (SA) in ALs has been shown to improve patient outcomes in cardiopulmonary bypass procedures.[8–11] Additionally, the ALs used for this application have been too bulky to allow for patient ambulation, which has been shown to be important in preparing patients for lung transplantation.[12,13] A wearable AL would be advantageous for children as a bridge to lung transplant because it would 1) supplement pulmonary function of the diseased native lungs; 2) facilitate ambulation during bridge to transplant or even as a destination device; 3) improve portability and reduce blood trauma by eliminating the need for a mechanical pump[14,15]; 4) avoid ventilator-associated events by allowing the patient to be extubated[2,16]; and 5) allow support outside of the intensive care unit (ICU) and even potentially outside of the hospital.

To function without a mechanical pump, the device and circuit must have a low enough resistance that the pressure gradient between the PA and LA, generated by the RV, is sufficient to drive adequate flow through the device. Assuming a mean PA pressure of at least 25 mm Hg (although hypertension in this patient population can produce mean PA pressures above 70 mm Hg)[17] and LA pressure of 10 mm Hg, the entire circuit (including MLung, tubing, and cannulas) must have a pressure drop less than 15 mm Hg; however, a circuit of even lower resistance is beneficial due to the alleviation of RV load. To meet the desired resistance of the entire circuit, our target for the Pediatric MLung itself is a pressure drop of 5 mm Hg at rated flow. Rated flow refers to the blood flow rate at which blood entering the device at an oxygen saturation (SO_2) of 70% exits the device at SO_2 of 95%.[18] The target rated flow for the Pediatric MLung is ≥0.75 L/min, which equates to up to 50 ml/min of oxygen transfer. This target is based on the oxygen demand of a typical pediatric patient[19] and would allow the Pediatric MLung to manage all the oxygenation of the patient if necessary.

The PA–LA attachment requires a device that has low resistance to flow. This can be problematic from a design perspective because device resistance increases with fiber number and density, both of which directly impact the gas exchange capability of the device. Additionally, current hollow fiber devices are limited by the “boundary layer effect” wherein the resistance to diffusion-based gas transfer is increased due to a plasma-rich layer devoid of red blood cells (RBCs) in close proximity to the fiber membranes.[20] To overcome this problem, researchers have investigated methods to induce secondary flows in the devices to disrupt the formation of this boundary layer.[20] These efforts include passive methods such as increasing the SA-to-volume (SA/V) ratio of the blood flow path (*i.e.*, microfluidic lungs), increasing flow velocity across the fiber bundle, including obstacles in the flow path, and

membrane texturing, and active methods such as building oxygenators with enclosed rotating discs and perfusing the devices with pulsatile flow.[21–25] Recently, we demonstrated a membrane lung based on a series of concentric gates, resulting in a circular blood flow path that induces secondary flows, disrupting the boundary layer, and improving overall gas exchange.[26] Based on our previous work, this study aims for designing a new AL that provides adequate gas exchange and pressure drop for pediatric patients.

Materials and Methods

Computational Fluid Dynamics

A solid three-dimensional (3D) model of the Pediatric MLung device was built in Solidworks (Dassault Systémes, Vélizy-Villacoublay, France), and computational fluid dynamics (CFD) simulation was carried out using Solidworks Flow Simulation add-in. The fiber bundle area was modeled as a continuous porous media. The resistance of the fiber bundle to be used in the porous media model was estimated using previous experimental data and equations 1–3,[27]

$$\Delta P = -\frac{\mu Q L}{\kappa A} \tag{1}$$

$$\kappa = \frac{\varepsilon^3 D_p^2}{A(1-\varepsilon)^2} \tag{2}$$

$$A = 497\varepsilon - 103 \tag{3}$$

where ΔP = pressure drop, μ = blood viscosity, Q = volumetric flow rate, L = blood path length, κ = fiber bundle permeability, ε = fiber bundle porosity, and D_p = effective particle diameter (estimated as 1.5 times the fiber diameter).[28]

To accurately model pressure drop within the fiber bundle, resistance data for the fiber bundle are typically determined by experimental measurements.[29] These measured values are then input into the porous media model. Data from our previous work were used to provide the necessary resistance data to simulate the fiber bundle as an isotropic porous media.[26] The experimental resistance data for the original fiber mat (17 fibers/cm) were scaled down linearly by multiplying by a factor (κ/κ_{LR}), where κ_{LR} is the predicted permeability of the low-resistance fiber mat (six fibers/cm) into equation 1. This provided the resistance data for the low-resistance fiber mat to be input into the porous media model for the CFD simulations.

Blood is modeled as a non-Newtonian fluid with a density of 1,060 kg/m^3. Viscosity is calculated using a power law model, with maximum dynamic viscosity of 0.012 Pa·s, minimum dynamic viscosity of 0.003 Pa·s, and power law index of 0.7991.

Boundary conditions were an inlet flow rate of 0.75 L/min at the device inlets (0.375 L/min at each inlet) and a pressure of 10 mm Hg at the device outlet. The automatic mesh function in Solidworks was used to generate the mesh, which has incremental settings between 1 and 7 (seven providing the most refined mesh). A grid independence study was performed which determined that the automatic mesh setting should be ≥3. Because of reasonable computational time (≈8 min), a mesh setting of 5 was used, which produced 356,686 fluid cells in the computational domain.

Basic Device Topology

The Pediatric MLung is composed of five housing parts, an inner and outer fiber bundle, and a liquid curing silicone (referred to as “potting”), which separates the blood and sweep gas flow paths. The Pediatric MLung components are a) outer housing (with blood inlets); b) gate insert; c) blood outlet; and d, e) two end caps (Figure 1). The fiber bundles are packed between the outer housing, gate insert, and blood outlet. The thicknesses of the inner and outer bundles are equivalent (2.3 cm). Two thirds of the total membrane SA is in the outer bundle, and one third is in the smaller inner bundle. The potting is applied to the ends of the fiber bundle as a liquid to fill in the tight spaces in between fibers. The potting then hardens at room temperature to form a barrier between the blood and gas phases to prevent blood leakage or air emboli formation in the blood.

MLung Fabrication

Three-dimensional computer-aided design (3D CAD) models of the housing components were built using Solidworks. Polyurethane housing components were injection molded (Stratasys Direct Manufacturing, Farmington Hills, Michigan). OXYPLUS polymethyl pentene (PMP) fiber mat (six fibers/cm) was obtained from 3M (St. Paul, Minnesota). Potting fixture components were 3D printed using M3 crystal resin and a Pro-Jet 3500 HD Max 3D printer (UM3D Lab, University of Michigan, Duderstadt Center, Ann Arbor, Michigan).

Polymethyl pentene fibers were hand-wound around the gate insert and blood outlet components (Figure 1) until snug within the fiber bundle area, taking care to prevent wrinkles in the fiber mat that would cause irregularity in the fiber bundle. The Pediatric MLung was then seated within a potting fixture, using temporary metal pins to suspend the gate insert to maintain proper alignment with the outer housing and blood outlet pieces during the potting process. A custom centrifuge was used to supply liquid silicone potting (Elastosil RT625; Wacker Chemie AG, Munich, Germany) to the ends of the fiber bundle. The silicone hardens at room temperature, whereas centrifugal force prevents liquid potting from creeping up the outsides of the fibers. To prevent creep of potting within the fiber lumens, the fiber ends were sealed using a heated metal edge before packing within the Pediatric MLung. Potting was introduced to the inlet reservoir tubing immediately after mixing (Figure 1). Devices were centrifuged for 2 hours and then allowed to sit overnight at room temperature. Devices were then removed from the potting fixture, and the excess potting was cut flush to the outer housing to expose the fiber lumens for sweep gas. End caps were affixed to the completed Pediatric MLungs.

Before benchtop performance testing or *in vivo* testing, the blood side of the Pediatric MLung was flushed with at least 1 L of sterile saline and then primed with sterile saline.

Benchtop Performance Testing

A benchtop flow circuit using slaughterhouse bovine blood was used to test gas exchange and pressure drop performance at various blood and sweep flow rates. Before bench testing, blood was filtered with a 32 μm mesh (Capiox arterial filter removed from a Capiox FX25 oxygenator, Terumo Cardiovascular Group, Ann Arbor, Michigan), preconditioned to standard venous values (per ISO7199/Food and Drug Administration [FDA] Guidelines[30]), and heparinized as necessary to an activated clotting time (ACT) >1,500 s. Heparinized blood from an inlet reservoir was directed to a centrifugal pump, which pumped blood to the test device and then to an outlet reservoir at programmed flow rates. Sweep gas was supplied to the Pediatric MLung from compressed gas tanks and controlled using a mass flow controller (Model MCP-50SLPM, D/10M; Alicat Scientific, Marana, Arizona). Sweep gas was supplied for each blood flow rate in a 2:1, 4:1, and 8:1 blood flow ratio. Blood flow rates of 0.5, 0.75, and 1 L/min were used. If device rated flow was either below 0.5 L/min or above 1 L/min, then blood flow rates of 0.25 or 1.25 L/min were added, respectively. Pre- and post-device blood gas samples were collected *via* sampling ports in the tubing and analyzed using a Radiometer ABL800flex blood gas analyzer (Radiometer, Brea, CA). Pre- and post-device blood-side pressure was monitored using Transpac disposable pressure transducers. Activated clotting time was measured using an Accriva Hemochron Response (Accriva, Bedford, MA) whole-blood coagulation system.

In Vivo Hemocompatibility and Performance Testing

All protocols were approved by the University of Michigan Committee on Care and Use of Animals, and animals received humane care in accordance with the National Institutes of Health Guide for the Care and Use of Laboratory Animals.

Healthy, fasted adult sheep (38–42 kg) was sedated using intravenous (IV) propofol (5–10 mg/kg) and intubated. General anesthesia was maintained using inhaled isoflurane (1–3.5%). The right femoral artery was accessed using 14 Fr Bio-medicus arterial cannula (Medtronic, Minneapolis, MN), and the right jugular vein was cannulated with a 20 Fr DLP venous cannula (Medtronic, Minneapolis, MN), both *via* cut-down technique. A femoral artery-to-jugular vein extracorporeal circuit was constructed, incorporating the Pediatric MLung. For experiments utilizing the PA–LA configuration, cannulation was performed through an end-to-side anastomosis with either polyester (polyester grafts: Vascutek, Inc; Renfrewshire, Scotland, UK) or polytetrafluoroethylene (PTFE grafts: Gore Medical; Newark, Delaware, USA). Occlusion of the right PA (rPA) was used as previously described as a disease model for ESLF.[5] The circuit was completely deaired and primed using approximately 200 ml sterile saline before opening arteriovenous flow. Solumedrol was administered (750 mg IV, 250 mg through the device inlet pressure port) immediately before opening blood flow to the Pediatric MLung circuit. This is done to prevent any acute allergic reaction from the sheep that could affect hemodynamics (which can occur because the devices are not sterile and there is a possibility of leaching of fabrication materials). Sheep were heparinized to an ACT consistent with clinical extracorporeal membrane oxygenation (ECMO) (ACT, 200–240 s).[31]

Before initiating shunt flow through the Pediatric MLung, minute ventilation was set to a standard baseline value of 7.2 L/min. Minute ventilation was reduced by 33% by decreasing respiratory rate to induce hypercapnia, and vecuronium bromide was administered (3 mg IV, subsequent IV drip at 1.5 mg/ml) to prevent spontaneous breathing of the animal with rising partial pressure of carbon dioxide in blood (PCO_2). When arterial PCO_2 reached a stable value (same PCO_2 for 15 min), arteriovenous blood flow was opened to the MLung circuit. Target arterial PCO_2 before initiating flow to the MLung was 50–60 mm Hg to test ventilation capability of the Pediatric MLung during hypercapnia. Sweep flow was controlled *via* mass flow controller (Model MCP-50SLPM, D/10M; Alicat Scientific), which was set at 6 L/min for the first hour, 12 L/min for the second hour, and 2 L/min for the remaining duration of the experiment. Blood flow rate through the device was monitored using a flow meter (Model T402; Transonic, Ithaca, New York) with flow probe (ME 9PXL; Transonic).

Blood gas samples, sweep gas exhaust samples, and ACT measurements were obtained every 15 min for 2 hours, then every 30 min for the duration of the experiment using a ABL800 Flex blood gas analyzer and Hemochron Response whole blood coagulation monitoring instrument (Accriva, Bedford, MA), respectively. Carbon dioxide (CO_2) removal was measured as fraction of CO_2 in the exhaust sweep gas. Complete blood count (CBC) samples were collected every hour throughout the experiment using a Procyte Dx hematology analyzer (IDEXX, Westbrook, ME). The experiment was concluded at 6 hours or when the device blood flow was reduced to less than 5% of initial flow due to clotting. Immediately upon conclusion of the experiments, the Pediatric MLung was removed from the circuit and flushed *via* gravity in the opposite direction of blood flow using sterile saline (at least 2 L) to remove any blood or clot nonadherent within the device and photographed to document any residual thrombi. After gross imaging, the intact units were flushed with 10% bleach (1–2 hours) followed by deionized water (overnight) and compressed air (overnight) to clean before use in future experiments.

Results

Computational Fluid Dynamics

The required gas exchange SA for the current device was estimated by scaling our previous design, which had a SA = 0.28 m^2 and a rated flow of 2 L/min, but a pressure drop of approximately 100 mm Hg.[26] Scaling down SA linearly (assuming equivalent gas exchange efficiency in the previous and new designs) gave a basis SA of 0.1 m^2 for the new design because this SA is expected to provide the necessary gas exchange to satisfy the rated flow requirement. Blood flow was simulated using the Solidworks Flow Simulation add-in (Dassault Systémes), and velocity and pressure profiles were generated (Figure 2).

At 0.75 L/min, pressure drop in a single-inlet MLung using a fiber mat with 17 fibers/cm and a fiber length of 2 cm was 38 mm Hg (from previous work).[26] To further reduce pressure drop, three changes were made from the previously published design (Table 1): 1) the use of a dual-inlet design; 2) fiber length increased to 3 cm; and 3) reduction of the fiber bundle porosity by using a low-density fiber mat (six fibers/cm). Each of these changes independently reduces pressure drop, and when the fiber bundle is modeled as an isotropic

porous media, a pressure drop of 2 mm Hg is predicted at a flow rate of 0.75 L/min. Six Pediatric MLungs were successfully fabricated as described in Methods and used for benchtop and *in vivo* testing.

Benchtop Testing

The Pediatric MLungs were performance tested using a previously described benchtop blood flow model.[26] Average rated flow of the six devices was 1 L blood/min (Figure 3). Average pressure drop (± standard error) at the target blood flow rate of 0.75 L/min was 18 ± 3 mm Hg, and at the achieved rated flow of 1 L/min was 25 ± 4 mm Hg. Average oxygenation rate and oxygenation efficiency were 45 ml/min and 350 ml/min/m^2 at rated flow, respectively.

In Vivo Testing and Hemocompatibility

The Pediatric MLungs were operated for 6 hours or until device flow was reduced to 5% of initial flow due to clotting (Figure 4). Average initial device flow (T0) was 0.8 ± 0.1 L/min (n = 3) at an average initial pressure drop of 11 ± 4 mm Hg. Devices A and B were used for the entire 6 hour experiment, and device C was used for 3.5 hours before the rapid decrease in blood flow (due to clotting) indicated an experimental end-point (device flow = 5% of initial flow). Flow resistance of the devices was initially 13 ± 3 mm Hg * min/L, which increases when clotting in the Pediatric MLung or blood circuit occurs (Figure 5). Six hours of device flow resulted in a 31% and 27% decrease in platelet count from the initial (T0) value for sheep with devices A and B attached, respectively, and a decrease in platelet count of 29% occurred within 3 hours in the device C sheep (Figure 6). White blood cell (WBC) count decreased by 34%, 0% (no change), and 8% in sheep attached to devices A, B, and C, respectively. Average CO_2 removal efficiency was initially 420 ± 42 ml/min/m^2 and gradually decreased throughout the course of the experiment (Figure 7). After the experiments, devices were rinsed with saline as described in Methods and imaged (see Supplemental Figure 1, http://links.lww.com/ASAIO/A433). Pediatric MLungs tested in the PA–LA configuration achieved a maximum of 0.383 ± 0.02 L/min of blood flow through the circuit without rPA occlusion and 0.617 ± 0.02 L/min of circuit flow with full occlusion of the rPA (Figure 8).

Discussion

Oxygenator geometry, blood path length, fiber length and number (gas exchange SA), and fiber bundle density together determine the pressure drop and gas exchange capability of the AL. Typically, ALs with high gas exchange capability also have a high pressure drop. By utilizing a concentric-gated design, circular flow induces mixing which improves the overall gas exchange efficiency. Additionally, the concentric gating increases the blood flow path length, increasing both gas exchange and pressure drop. We offset this increase in pressure drop by utilizing 1) a dual-inlet design and 2) a low-density fiber mat. The dual-inlet design reduces resistance by splitting the flow, effectively shortening the average blood path length but maintaining the benefit of the concentric gating. This is evidenced in that the oxygenation efficiency in the Pediatric MLung is the same as the single-inlet MLung, in which the blood path length is roughly twice as long. The low-density fiber mat provides a fiber bundle with lower resistance. The resulting device meets the gas exchange

specification, but operates above the target pressure drop. The current device still is clinically relevant in its current design because hypertensive patients may produce PA pressures above 70 mm Hg.[17] However, changes will be made to future iterations of the device to achieve target pressure drop to allow treatment of normotensive patients and reduce RV load.

Gas exchange performance is comparable to our previous published AL design and is more efficient than current clinical devices (Table 2). Priming volume is comparable to clinical pediatric ALs but will be reduced in future designs by making devices which are smaller in size but use a higher density fiber mat to meet specifications. Increasing the density of the fiber mat will increase pressure drop, but this will be offset by tuning other parameters such as fiber length and the length of the blood flow path. Carbon dioxide removal efficiency gradually decreased throughout the course of the experiment, likely due to an increase in the resistance to CO_2 diffusion caused by water condensation in the gas phase, platelet deposition on the fiber surface, or a combination of both.

The pressure drop of the Pediatric MLungs was higher than predicted by CFD simulations. Slight differences between the intended and actual Pediatric MLung parameters (2.5 ± 0.1 cm fibers rather than 3 cm, 0.13 m^2 membrane SA rather than 0.10, porosity of 0.86 rather than 0.9) account for some of this difference in pressure drop. However, when these values are reflected in the simulations, CFD still predicts a lower pressure drop than what was experimentally observed. In the simulation, the fiber bundle is treated as a continuous, isotropic porous media rather than a collection of discrete fiber bundles. In practice, the fiber bundles have different permeabilities depending on the direction of blood flow. Additionally, the fibers in the device are not equally spaced. Although each adjacent fiber is equally spaced within the fiber mat (*i.e.*, in the circumferential direction in the fiber bundle), as the fiber bundle is wrapped, the adjacent fibers in the radial direction are much closer together. This causes the estimated permeability to be different from the actual permeability of the non-homogenous fiber mat. In this cylindrical configuration, the fiber bundle is more accurately modeled as an axisymmetric or anisotropic porous media[36]; however, the resistance in each direction across the fiber bundle must be determined experimentally to accurately model the fiber bundle as an axisymmetric or anisotropic porous media.

Two Pediatric MLungs demonstrated use in the arteriovenous circuit over 6 hours and a third was used for 3.5 hours before clotting in the circuit caused flow to drop substantially. Platelet consumption was gradual but apparent in the three devices tested (31%, 27%, and 29% reduction in platelet count for devices A, B, and C, respectively), whereas a consistent trend regarding WBC concentration was not apparent. The clotting that was observed qualitatively occurred in three areas: 1) an area of apparent recirculating flow in the inlet of the device; 2) along the horizontal cross-threads that hold the fiber mat together; and 3) at areas adjacent to the potting (see, Supplemental Figure 1, http://links.lww.com/ASAIO/A433). Future designs will include refinement of the inlet geometry to remove the area of recirculating flow. The fiber crossthreads are necessary for the integrity of the fiber mat but can potentially be situated to be present only within the potting of the device and not in the active blood-contacting region. Longer-term animal studies are necessary to verify hemocompatibility for chronic applications. In this work, acute hemocompatibility/

thrombosis is evaluated without the aid of nonthrombogenic coatings/sweep gas additives. However, future iterations of the Pediatric MLung including chronic hemocompatibility testing will incorporate a nonthrombogenic coating and the addition of nitric oxide to the sweep gas.

Much of the current work focuses on designing the Pediatric MLung, so that it has a low resistance. Although resistance is the opposition to steady flow, impedance can be thought of as the opposition to pulsatile flow.[37,38] Impedance is determined by both the resistance and compliance of the circuit (as well as parameters related to the fluid and pulsatility).[39,40] Circuit compliance is an important consideration that has been shown to affect cardiac function and RV load, particularly for long-term support.[41] This is seen in normal, healthy pulmonary circulation as well. In addition to having low resistance to steady flow (relative to systemic arterial circulation), the natural pulmonary circulation displays enhanced vascular distention (compliance) which is important in allowing pressures in these vessels to remain low.[37,42] Artificial lungs that have higher than physiologic impedances can produce abnormal pulmonary hemodynamics when connected in parallel or in series with the natural lung.[43] Compliant ALs and circuits have been developed to achieve impedances even lower than the natural lung.[44–46] Circuit compliance will be an important consideration for the development and implementation of the Pediatric MLung; however, in this work, we have focused solely on the resistance aspect of the AL. Future work will done to incorporate the proper level of compliance to the circuit.

In conclusion, a pediatric AL based on concentric gating (Pediatric MLung) was designed and fabricated. The device has a rated blood flow of 1 L/min and a pressure drop = 25 mm Hg at rated flow. A dual-inlet design and low-resistance fiber mat was used to keep pressure drop low while maintaining adequate gas exchange capability. We demonstrated repeatable fabrication (n = 6), confirmed performance in benchtop blood flow testing and in an acute sheep model of ECMO. The next step for this work will be implantation of the device in a chronic sheep model to demonstrate long-term pulmonary support.

Supplementary Material

Refer to Web version on PubMed Central for supplementary material.

Acknowledgment

The authors thank all of the University of Michigan Extracorporeal Life Support (ECLS) Laboratory technicians, fellows, Undergraduate Research Opportunity Program students, Surgery 499 students, and volunteers who have helped with this work. In particular, the authors thank Mark Langley, Felicia Hinojosa, Rami Beydoun, and Devak Nanua for their help with *in vivo* experiments. The authors Cindy Cooke for her support of this work, in particular with the preparation of grant proposals and manuscripts.

This work was supported by the National Institutes of Health grant 2R01 HD015434-34.

References

1. Valapour M, Skeans MA, Smith JM, et al.: OPTN/SRTR 2015 annual data report: lung. Am J Transplant 17(suppl 1): 357–424, 2017. [PubMed: 28052607]

2. Alghanem F, Davis RP, Bryner BS, et al.: The implantable pediatric artificial lung: interim report on the development of an end-stage lung failure model. ASAIO J 61: 453–458, 2015. [PubMed: 25905495]

3. Boston US, Fehr J, Gazit AZ, Eghtesady P: Paracorporeal lung assist device: an innovative surgical strategy for bridging to lung transplant in an infant with severe pulmonary hypertension caused by alveolar capillary dysplasia. J Thorac Cardiovasc Surg 146: e42–e43, 2013. [PubMed: 23871141]

4. Hoganson DM, Gazit AZ, Boston US, et al.: Paracorporeal lung assist devices as a bridge to recovery or lung transplantation in neonates and young children. J Thorac Cardiovasc Surg 147: 420–426, 2014. [PubMed: 24199759]

5. Alghanem F, Bryner BS, Jahangir EM, et al.: Pediatric artificial lung: a low-resistance pumpless artificial lung alleviates an acute lamb model of increased right ventricle afterload. ASAIO J 63: 223–228, 2017. [PubMed: 27861431]

6. Hoganson DM, Gazit AZ, Sweet SC, Grady RM, Huddleston CB, Eghtesady P: Neonatal paracorporeal lung assist device for respiratory failure. Ann Thorac Surg 95: 692–694, 2013. [PubMed: 23336880]

7. Gazit AZ, Sweet SC, Grady RM, Huddleston CB: First experience with a paracorporeal artificial lung in a small child with pulmonary hypertension. J Thorac Cardiovasc Surg 141: e48–e50, 2011. [PubMed: 21420104]

8. Hsu LC: Biocompatibility in cardiopulmonary bypass. J Cardiothorac Vasc Anesth 11: 376–382, 1997. [PubMed: 9161907]

9. Cormack JE, Forest RJ, Groom RC, Morton J: Size makes a difference: use of a low-prime cardiopulmonary bypass circuit and autologous priming in small adults. Perfusion 15: 129–135, 2000. [PubMed: 10789567]

10. Jansen PG, te Velthuis H, Bulder ER, et al.: Reduction in prime volume attenuates the hyperdynamic response after cardiopulmonary bypass. Ann Thorac Surg 60: 544–549, 1995; discussion 549. [PubMed: 7677478]

11. Shapira OM, Aldea GS, Treanor PR, et al.: Reduction of allogeneic blood transfusions after open heart operations by lowering cardiopulmonary bypass prime volume. Ann Thorac Surg 65: 724–730, 1998. [PubMed: 9527202]

12. Rehder KJ, Turner DA, Hartwig MG, et al.: Active rehabilitation during extracorporeal membrane oxygenation as a bridge to lung transplantation. Respir Care 58: 1291–1298, 2013. [PubMed: 23232742]

13. Olsson KM, Simon A, Strueber M, et al.: Extracorporeal membrane oxygenation in nonintubated patients as bridge to lung transplantation. Am J Transplant 10: 2173–2178, 2010. [PubMed: 20636463]

14. Fraser CD Jr, Jaquiss RD, Rosenthal DN, et al.; Berlin Heart Study Investigators: Prospective trial of a pediatric ventricular assist device. N Engl J Med 367: 532–541, 2012. [PubMed: 22873533]

15. Chen JM, Richmond ME, Charette K, et al.: A decade of pediatric mechanical circulatory support before and after cardiac transplantation. J Thorac Cardiovasc Surg 143: 344–351, 2012. [PubMed: 22143101]

16. Elizur A, Sweet SC, Huddleston CB, et al.: Pre-transplant mechanical ventilation increases short-term morbidity and mortality in pediatric patients with cystic fibrosis. J Heart Lung Transplant 26: 127–131, 2007. [PubMed: 17258145]

17. Berger RM, Beghetti M, Humpl T, et al.: Clinical features of paediatric pulmonary hypertension: a registry study. Lancet 379: 537–546, 2012. [PubMed: 22240409]

18. Federspiel WJ, Henchir KA: Lung, artificial: basic principles and current applications, in Bowlin GL, Wnek G (eds), Encyclopedia of Biomaterials and Biomedical Engineering,. New York, Marcel Dekker, 2004, pp. 910–921.

19. McMurray RG, Butte NF, Crouter SE, et al.; CDC/NCI/NCCOR Research Group on Energy Expenditure in Children: Exploring metrics to express energy expenditure of physical activity in youth. PLoS One 10: e0130869, 2015. [PubMed: 26102204]

20. Wegner JA: Oxygenator anatomy and function. J Cardiothorac Vasc Anesth 11: 275–281, 1997. [PubMed: 9161895]

21. Richardson PD, Galletti PM: Correlation of effects of blood flow rate, viscosity and design features on artificial lung performance, in Dawids SG, Engell HC (eds), Physiological and Clinical Aspects of Oxygenator Design. Amsterdam, Netherlands, Elsevier, 1976, pp. 29–44.
22. Tanishita K, Nakano K, Richardson PD, Galletti PM, Sugawara M, Sakurai Y: Augmentation of gas transfer with pulsatile flow in the coiled tube membrane oxygenator design. Trans Am Soc Artif Intern Organs 26: 561–566, 1980. [PubMed: 7245549]
23. Bellhouse BJ, Bellhouse FH, Curl CM, et al.: A high efficiency membrane oxygenator and pulsatile pumping system, and its application to animal trials. Trans Am Soc Artif Intern Organs 19: 72–79, 1973. [PubMed: 4722780]
24. Moss RA, Benn JA, Ghadar FK, Drinker PA: Secondary flow and mass transfer in an oscillating torus Adv Cardiol 6: 40–55, 1971.
25. Schraven L, Kaesler A, Flege C, et al.: Effects of pulsatile blood flow on oxygenator performance. Artif Organs 42: 410–419, 2018. [PubMed: 29436001]
26. Fernando UP, Thompson AJ, Potkay J, et al.: A membrane lung design based on circular blood flow paths. ASAIO J 63: 637–643, 2017. [PubMed: 28665829]
27. Madhani SP, D'Aloiso BD, Frankowski B, Federspiel WJ: Darcy permeability of hollow fiber membrane bundles made from membrana polymethylpentene fibers used in respiratory assist devices. ASAIO J 62: 329–331, 2016. [PubMed: 26809086]
28. Pacella HE, Eash HJ, Federspiel WJ: Darcy permeability of hollow fiber bundles used in blood oxygenation devices. J Memb Sci 382: 238–242, 2011. [PubMed: 22927706]
29. Schlanstein PC, Limper A, Hesselmann F, Schmitz-Rode T, Steinseifer U, Arens J: Experimental method to determine anisotropic permeability of hollow fiber membrane bundles J Memb Sci 546: 70–81, 2018.
30. Guidance for Cardiopulmonary Bypass Oxygenators 510(k) Submissions; Final Guidance for Industry and FDA Staff. 2000 Available at: https://www.fda.gov/regulatory-information/search-fda-guidance-documents/guidance-cardiopulmonary-bypass-oxygenators-510k-submissions-final-guidance-industry-and-fda-staff.
31. Extracorporeal Life Support Organization: ELSO Anticoagulation Guideline: ELSO Guidel. 2014 Available at: https://www.elso.org/Portals/0/Files/elsoanticoagulationguideline8-2014-table-contents.pdf. Accessed March 7, 2018.
32. Sun L, Kaesler A, Fernando P, Thompson AJ, Toomasian JM, Bartlett RH: CO2 clearance by membrane lungs. Perfusion 33: 249–253, 2018. [PubMed: 29090614]
33. Wei X, Sanchez PG, Liu Y, et al.: Extracorporeal respiratory support with a miniature integrated pediatric pump-lung device in an acute ovine respiratory failure model. Artif Organs 40: 1046–1053, 2016. [PubMed: 27087252]
34. Orizondo RA, May AG, Madhani SP, et al.: In vitro characterization of the pittsburgh pediatric ambulatory lung. ASAIO J 64: 806–811, 2018. [PubMed: 29240630]
35. May AG, Orizondo RA, Frankowski BJ, Wearden PD, Federspiel WJ: Acute in vivo evaluation of the pittsburgh pediatric ambulatory lung. ASAIO J 65: 395–400, 2019. [PubMed: 30507846]
36. Bhavsar SS, Schmitz-Rode T, Steinseifer U: Numerical modeling of anisotropic fiber bundle behavior in oxygenators. Artif Organs 35: 1095–1102, 2011. [PubMed: 21973082]
37. Milnor WR: Pulsatile blood flow. N Engl J Med 287: 27–34, 1972. [PubMed: 4555147]
38. Haft JW, Bull JL, Rose R, et al.: Design of an artificial lung compliance chamber for pulmonary replacement. ASAIO J 49: 35–40, 2003. [PubMed: 12558305]
39. McGillicuddy JW, Chambers SD, Galligan DT, Hirschl RB, Bartlett RH, Cook KE: In vitro fluid mechanical effects of thoracic artificial lung compliance. ASAIO J 51: 789–794, 2005. [PubMed: 16340369]
40. Haft JW, Alnajjar O, Bull JL, Bartlett RH, Hirschl RB: Effect of artificial lung compliance on right ventricular load. ASAIO J 51: 769–772, 2005. [PubMed: 16340366]
41. Sato H, Hall CM, Lafayette NG, et al.: Thirty-day in-parallel artificial lung testing in sheep. Ann Thorac Surg 84: 1136–1143, 2007; discussion 1143. [PubMed: 17888959]
42. Kussmaul WG, Noordergraaf A, Laskey WK: Right ventricular-pulmonary arterial interactions. Ann Biomed Eng 20: 63–80, 1992. [PubMed: 1562105]

43. Schewe RE, Khanafer KM, Orizondo RA, Cook KE: Thoracic artificial lung impedance studies using computational fluid dynamics and in vitro models. Ann Biomed Eng 40: 628–636, 2012. [PubMed: 22009316]

44. Scipione CN, Schewe RE, Koch KL, Shaffer AW, Iyengar A, Cook KE: Use of a low-resistance compliant thoracic artificial lung in the pulmonary artery to pulmonary artery configuration. J Thorac Cardiovasc Surg 145: 1660–1666, 2013. [PubMed: 23402692]

45. Schewe RE, Khanafer KM, Arab A, Mitchell JA, Skoog DJ, Cook KE: Design and in vitro assessment of an improved, low-resistance compliant thoracic artificial lung. ASAIO J 58: 583–589, 2012. [PubMed: 23103694]

46. Akay B, Foucher JA, Camboni D, Koch KL, Kawatra A, Cook KE: Hemodynamic design requirements for in-series thoracic artificial lung attachment in a model of pulmonary hypertension. ASAIO J 58: 426–431, 2012. [PubMed: 22581034]

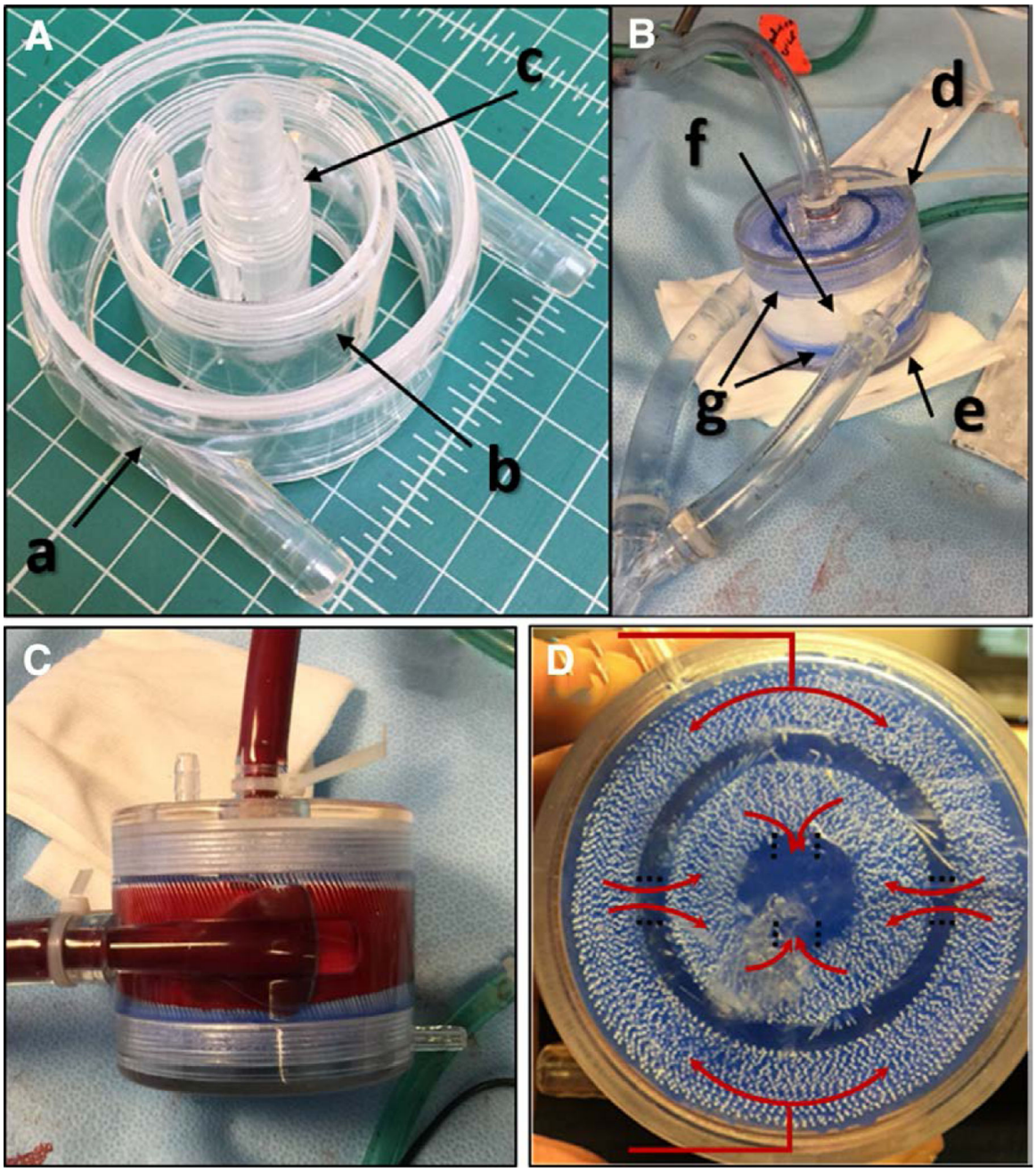

Figure 1.

Basic device topology of the Pediatric MLung. **A**, **B**: The components the comprise the device include (a) outer housing, (b) gate insert, (c) blood outlet, (d, e) end caps, (f) fiber bundles, and (g) the blue silicone potting. **C**: Side view of a Pediatric MLung; the fibers are oriented vertically within the housing in this image. **D**: Top view of a Pediatric MLung with illustration of the blood flow paths (red arrows).

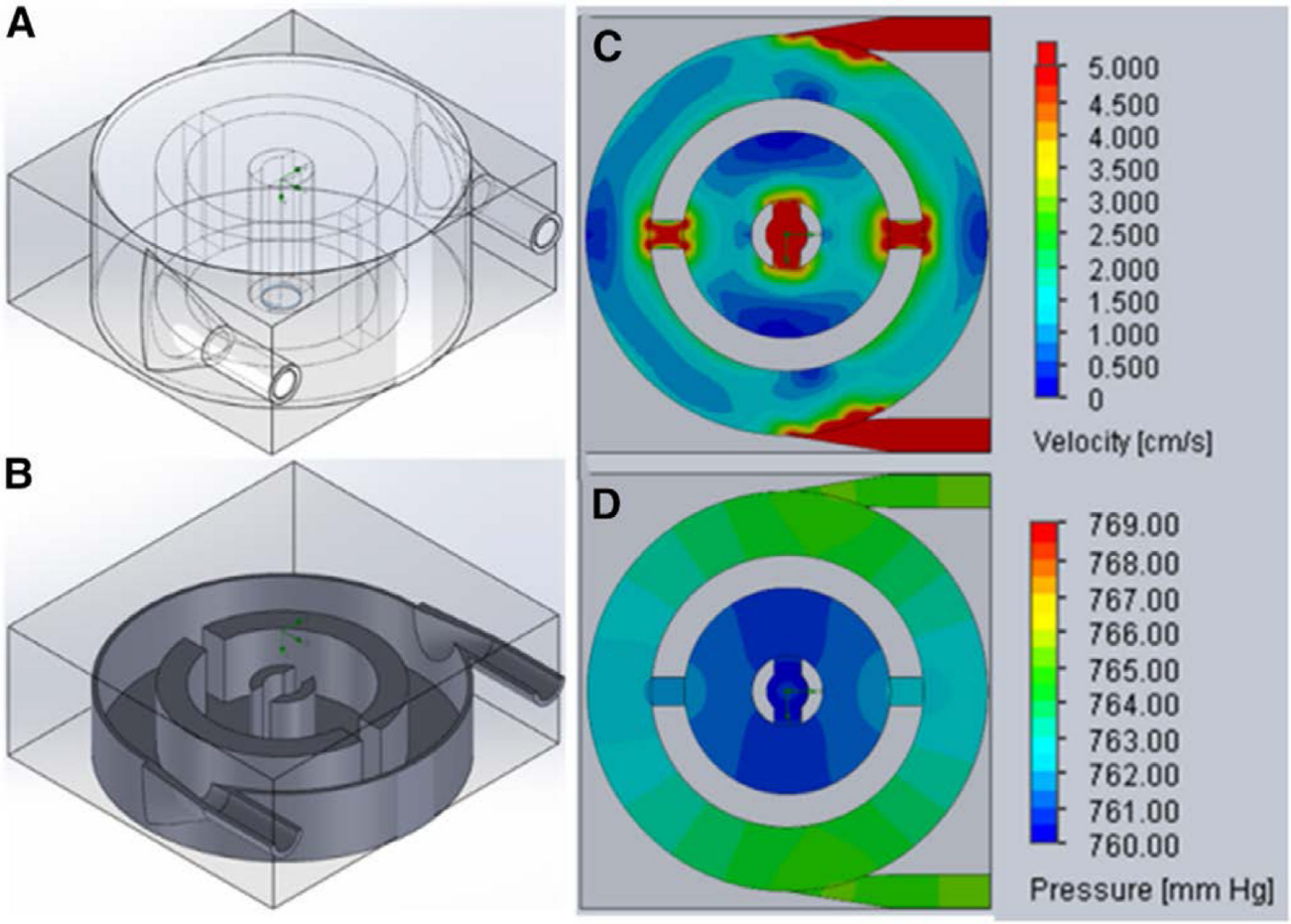

Figure 2.

Isometric views of the 3D model (**A**) and a cross-section through a midplane (**B**) of the pediatric MLung having 3 cm fiber length. Velocity (**C**) and pressure (**D**) profiles through the mid-plane of the Pediatric MLung were generated with Solidworks Flow Simulation. 3D, three-dimensional.

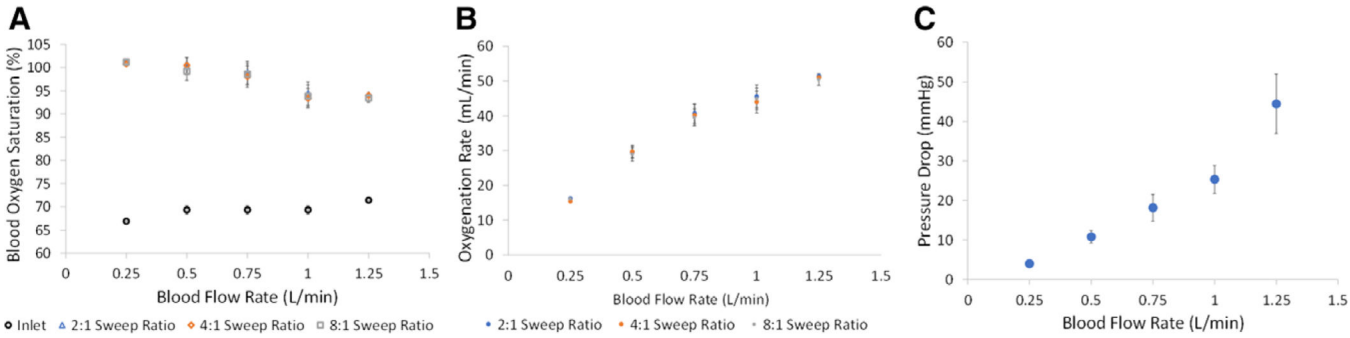

Figure 3.

Oxygenation (**A**, **B**) and pressure drop (**C**) of pediatric MLung during benchtop blood flow testing (n = 6).

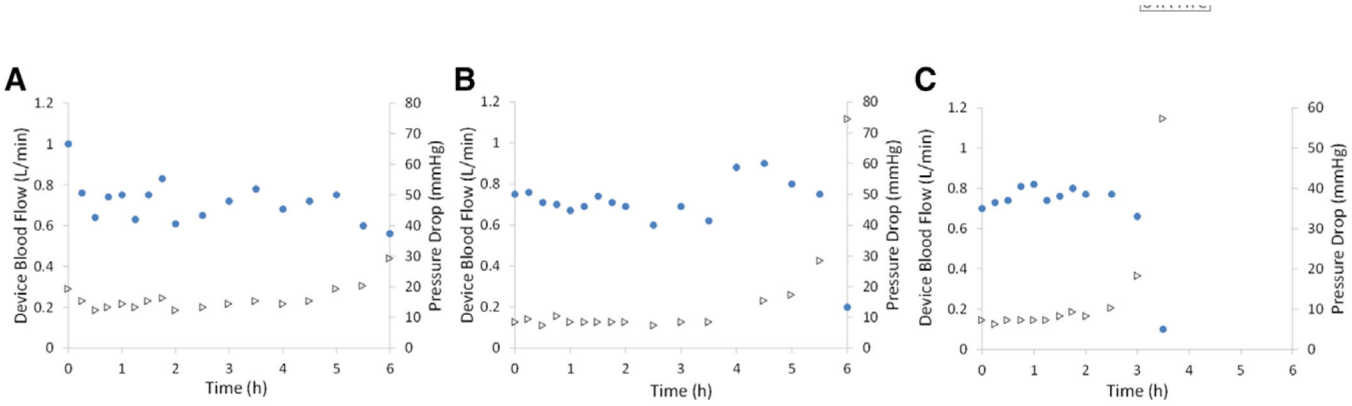

Figure 4.

Device flow rate (circles) and corresponding pressure drop (triangles) during 6 hours of arteriovenous blood flow from adult sheep. Three Pediatric MLungs were tested (**A**–**C**) for 6 hours or until device flow was reduced to 5% of initial flow.

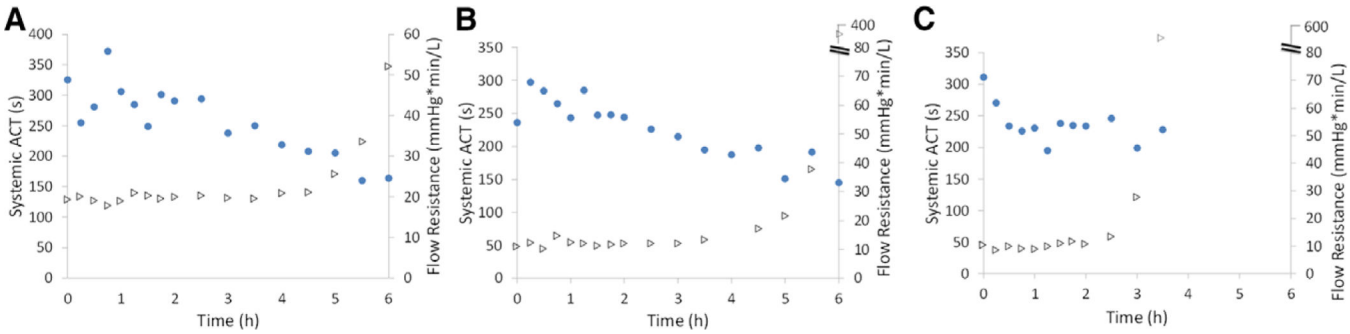

Figure 5.

Systemic ACT (circles) and device resistance (triangles) during 6 hours of arteriovenous blood flow from adult sheep. Three Pediatric MLungs were tested (**A**–**C**) for 6 hours or until device flow was reduced to 5% of initial flow. ACT, activated clotting time.

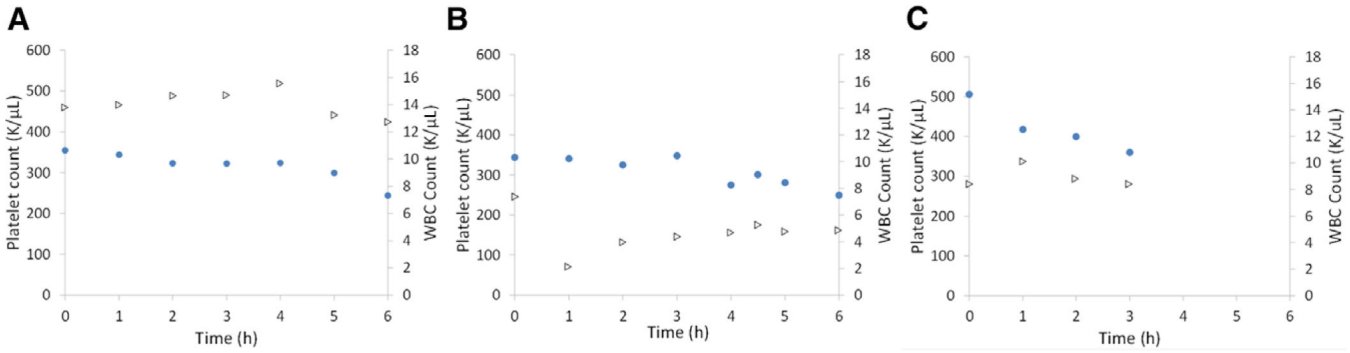

Figure 6.

Platelet count (circles) and WBC count (triangles) during 6 hours of arteriovenous blood flow from adult sheep. Three Pediatric MLungs were tested (**A**–**C**) for 6 hours or until device flow was reduced to 5% of initial flow. WBC, white blood cell.

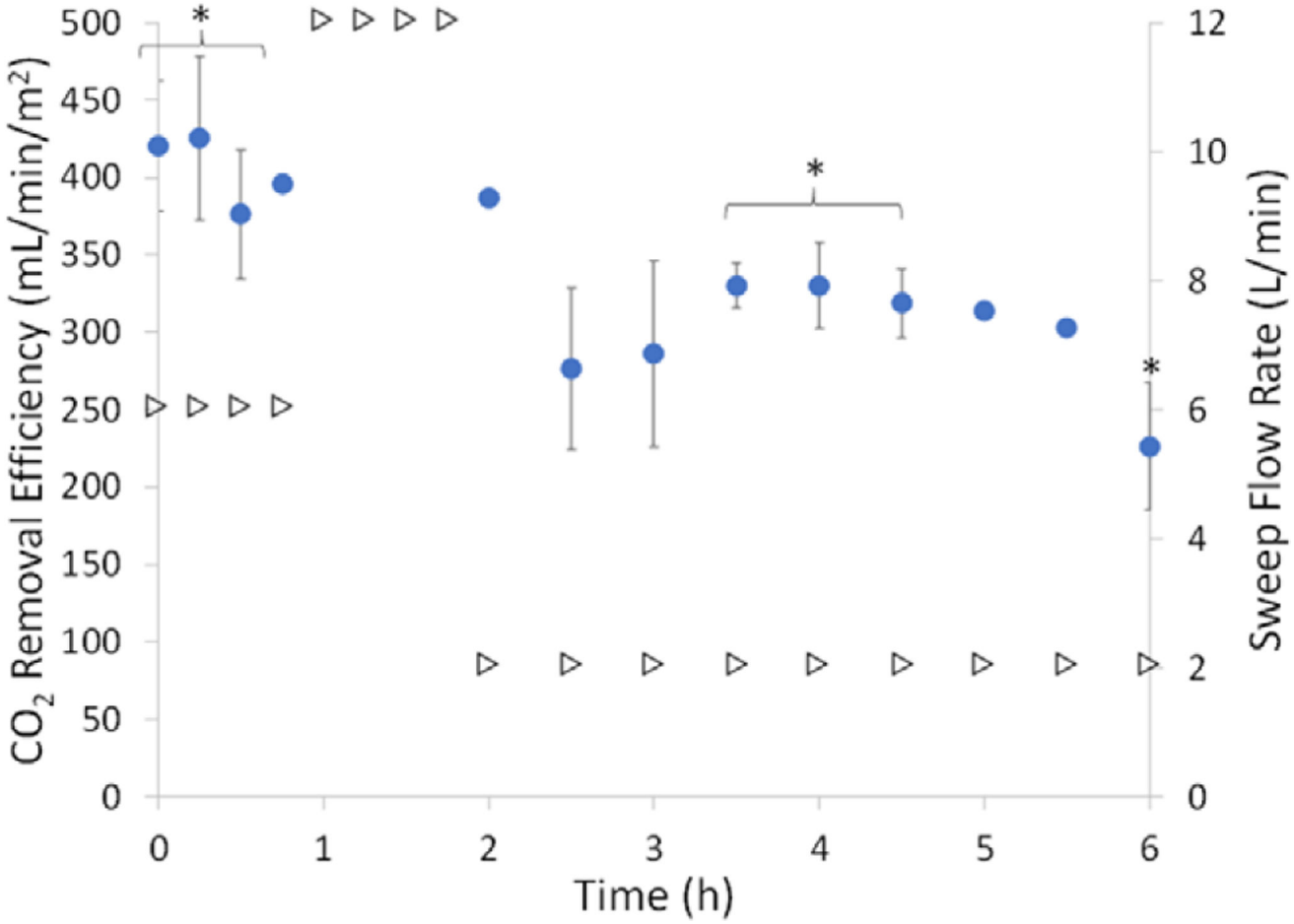

Figure 7.

CO_2 removal efficiency (circles) at varied sweep flow (triangles) of three Pediatric MLungs that were tested for 6 hours or until device flow was reduced to 5% of initial flow. Datapoints not gathered were due to dilution of the sample by sweep gas making the collected CO_2 concentration below the detection limit of the blood gas machine (average ± SEM, n = 3, *n = 2, no error bar: n = 1). CO_2, carbon dioxide; SEM, standard error mean.

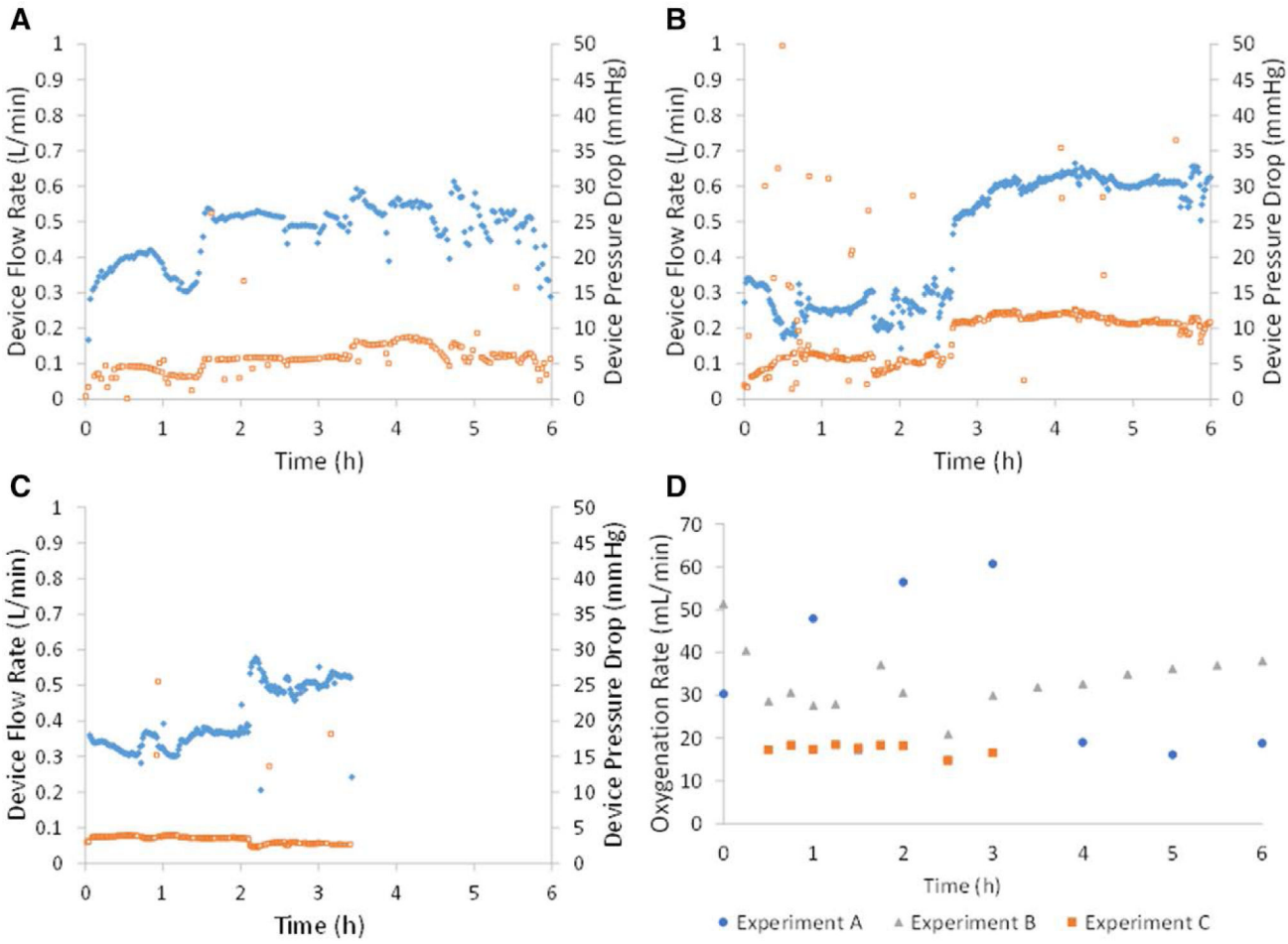

Figure 8.

Device flow rate (diamonds) and corresponding pressure drop (squares) during 6 hours of blood flow from adult sheep. Three Pediatric MLungs were tested (**A**–**C**) for 6 hours (with exception of plot C, in which the experiment was ended voluntarily after occlusion of the rPA did not result in blood flow of at least 0.75 L/min). Oxygenation rate was measured throughout each experiment (**D**). rPA, right pulmonary artery.

Table 1.

Computational Fluid Dynamics-Predicted Pressure Drop and Shear Stress in the Pediatric MLung Using Target Values for Fiber Length, Porosity, and Surface Area (Bold)

Inlet Configuration	Porosity	κ (cm^2)	Fiber Length (cm)	Fiber Mat Density (Fiber/cm)	Surface Area (m^2)	Pressure Drop (mm Hg)	Shear Stress (dyn/cm^2)	
							Max	Average
Single inlet[26]	0.58	2×10^{-9}	2	17	0.28	38 *	-	-
Dual inlet (target)	**0.9**	**7×10^{-8}**	**3**	**6**	**0.10**	**4.03**	**53**	**8.3**
Dual inlet (measured)	*0.85 ± 0.003*	*3×10^{-8}*	*2.5 ± 0.3*	*6*	*0.13 ± 0.02*	8.71 †	67 †	7.0 †

After fabricating devices (n = 6), the simulation was run using experimentally achieved values (italics; average ± SD, n = 6) for fiber length, porosity, and surface area in the fabricated devices.

*Experimentally measured data.[26]

†Pressure and shear values for the fabricated devices are from CFD simulation using the achieved fiber length and porosity values.

CFD, computational fluid dynamics; SD, standard deviation.

Table 2.

Comparison of Pediatric MLung to Current Devices in Clinical Use and Next Generation Devices in the Literature

Comparison Between MLung and Commercial Oxygenators						
					Gas Exchange Efficiency at Rated Flow (mL/min/m^2)	
Device	**Surface Area (m^2)**	**Rated Flow (L/min)**	**Pressure Drop at Rated Flow (mm Hg)**	**Priming Volume (mL)**	**O_2**	**CO_2**
Terumo Capiox RX05 (Terumo Cardiovascular Group, Ann Arbor, Michigan)	0.5	1.5	110	43	150	500 *
Maquet Quadrox Neonatal (Maquet, Rastatt, Germany)	0.38	1.5	58	40	197	189
Maquet Quadrox Pediatric (Maquet, Rastatt, Germany)	0.8	2.8	60 (1.5 L/min)	99	175	250
Sorin Dideco D100 (Sorin Group, Saluggia, Italy)	0.22	0.7	175	47	159	145
Novalung ILA (Xenios AG, Heilbronn, Germany)	1.3	Data not available †	Data not available	175	85 †	212 †
Pedipump Lung (University of Maryland, Baltimore, Maryland)	0.3	2.5	150	110	400	343 ‡
P-PAL (University of Pittsburgh, Pittsburgh, Pennsylvania)	0.3	Data not available §	Data not available §	270 §	310 §	Data not available
MLung (single inlet); (University of Michigan, Ann Arbor, Michigan)	0.28	2.0	106	47	357	714
Pediatric MLung (University of Michigan, Ann Arbor, Michigan)	0.13	1.0	25	68 ± 7	349	343 ± 90 ¶

Data for commercial devices were gathered from manufacturers technical information available *via* company websites.

*Capiox RX05 CO_2 removal data were estimated from Sun *et al.*[32]

†Novalung iLA is designed for CO_2 removal, and data at rated flow were not available; therefore, the CO_2 removal at the maximum flow for which data were available was reported.

‡CO_2 exchange efficiency for the Pedipump Lung was estimated from Wei *et al.*[33]

§Rated flow was not reported for the P-PAL; however, gas exchange efficiency was comparable to the PediPL at a flow rate of 2 L/min.[33,34] Priming volume of the P-PAL circuit is reported which includes fiber bundle area, pump area, and conduits.[35] Pressure drop of gas exchange region not reported; this device incorporates a pump to generate pressure and is intended for venoarterial use. CO_2 removal data not reported.

¶CO_2 exchange efficiency was taken as the average of the highest values achieved during *in vivo* testing (n = 3).

CO_2, carbon dioxide; O_2, oxygen.